Electronic Supplementary Information for

CoFe Prussian Blue Analogues on 3D Porous N-doped Carbon Nanosheet Boost the Intercalation Kinetics for High-Performance Quasi-Solid-State Hybrid Capacitor

Juhyung Choi,[a,‡] Jiho Lim,[a,‡] Daekyu Kim,[b] Sumin Park,[a] Bingyi Yan,[a] Dongjin Ko,[a] Youngseul Cho,[a] Lawrence Yoon Suk Lee,[b,] and Yuanzhe Piao[a,c,]**

[a] Department of Transdisciplinary Studies, Graduate School of Convergence Science and Technology, Seoul National University, 145 Gwanggyo-ro, Yeongtong-gu, Suwonsi, Gyeonggi-do, 16229, Republic of Korea

[b] Department of Applied Biology and Chemical Technology and Research Institute for Smart Energy, The Hong Kong Polytechnic University, Hung Hom, Kowloon, Hong Kong SAR, China

[c] Advanced Institutes of Convergence Technology, 145 Gwanggyo-ro, Yeongtong-gu, Suwon-si, Gyeonggi-do, 16229, Republic of Korea

‡ These authors equally contributed to this work.

Corresponding authors: lawrence.ys.lee@polyu.edu.hk (L.Y.S. Lee); parkat9@snu.ac.kr (Y. Piao).

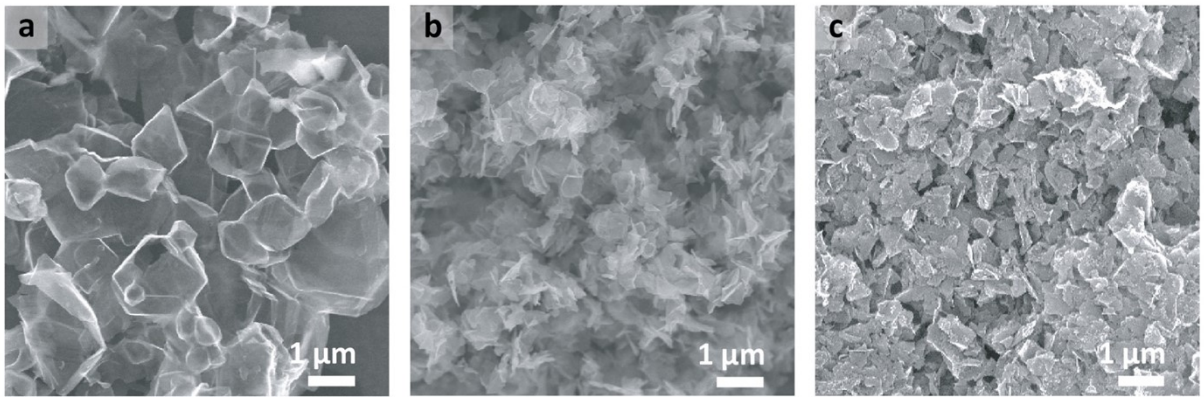

Fig. S1. SEM images of (a) IPC, (b) IPNC, and (c) CoFe PBA/IPNC.

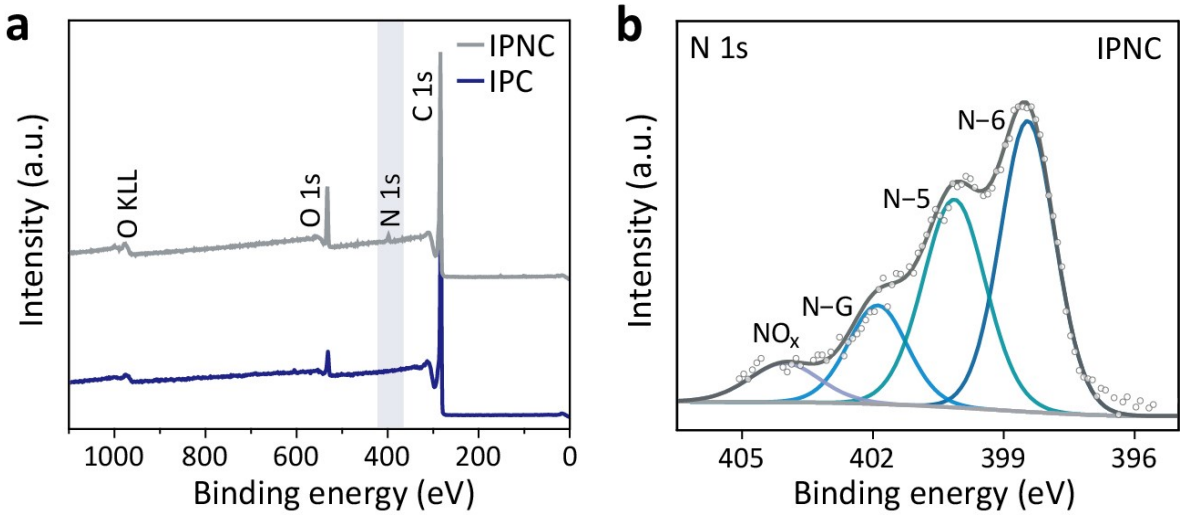

Fig. S2. (a) XPS survey spectra of IPNC and IPC and (b) high-resolution N 1s spectrum of IPNC.

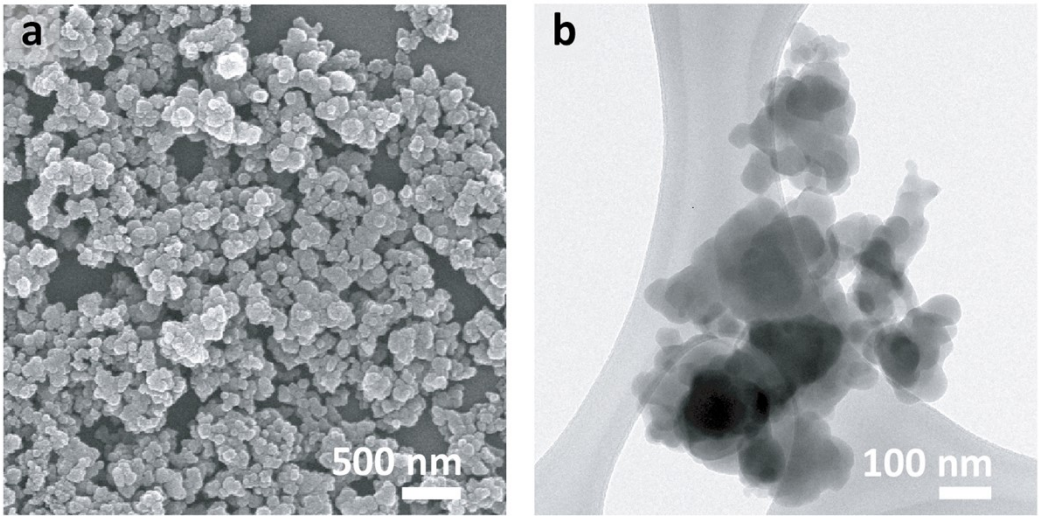

Fig. S3. (a) SEM and (b) TEM image of CoFe PBA nanoparticles.

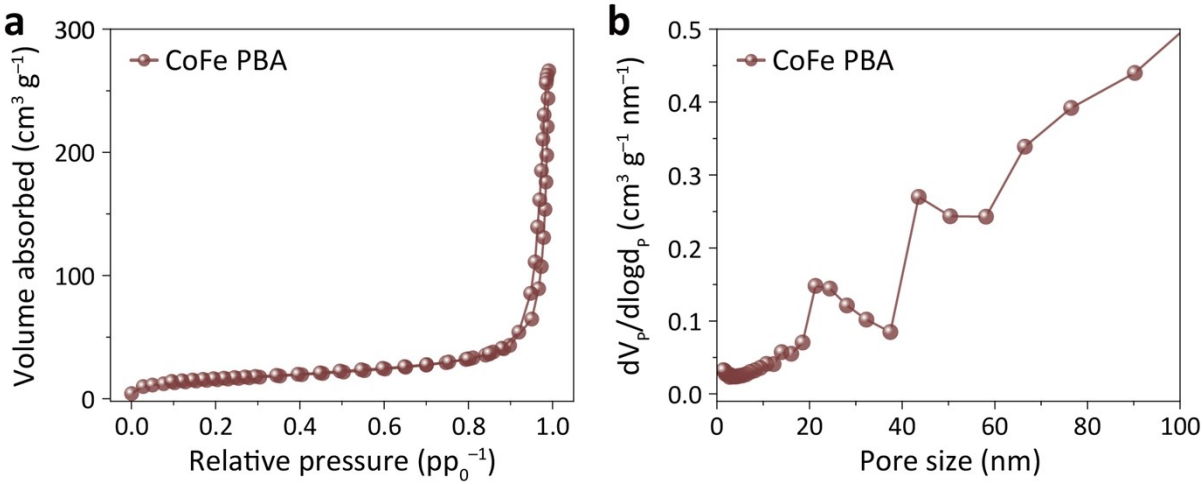

Fig. S4. (a) N_2 adsorption–desorption isotherms and (b) size distribution of CoFe PBA obtained using the Barrett–Joyer–Halenda (BJH) method.

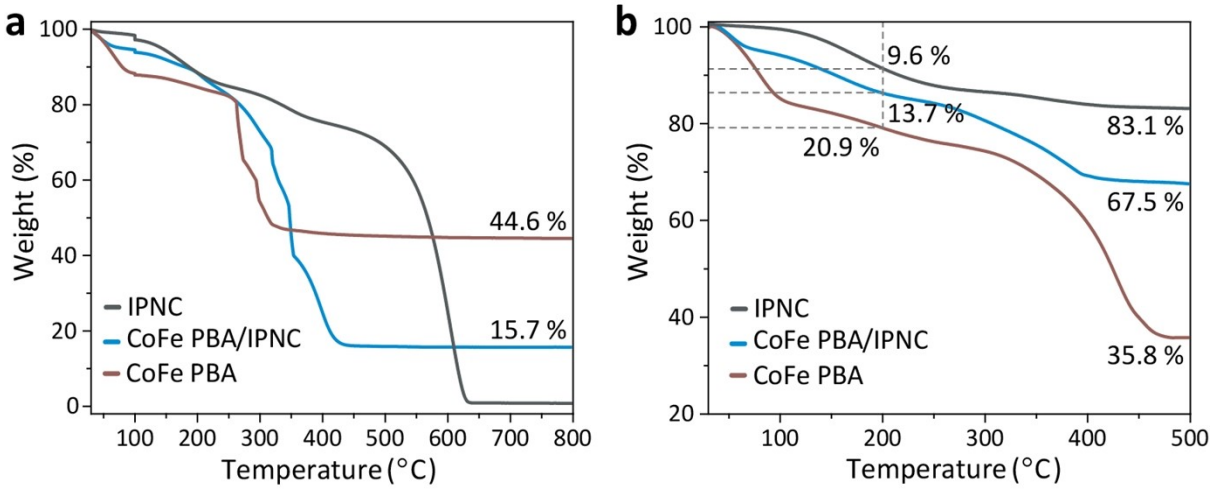

Fig. S5. Thermal gravimetric analysis (TGA) curves of IPNC, CoFe PBA/IPNC, and CoFe PBA obtained under (a) air and (b) Ar atmosphere at a ramping rate of 10 °C min^{-1}.

According to the TGA analysis in the air atmosphere, the remaining mass percentage is 44.6, 15.7, and 0 % for CoFe PBA, CoFe PBA/IPNC, and IPNC, respectively (**Fig. S5a**). Assuming the complete conversions of CoFe PBA to $CoFe_2O_4$ and IPNC to CO_2, the mass percentage of CoFe PBA in the CoFe PBA/IPNC can be estimated as 35.2 %.

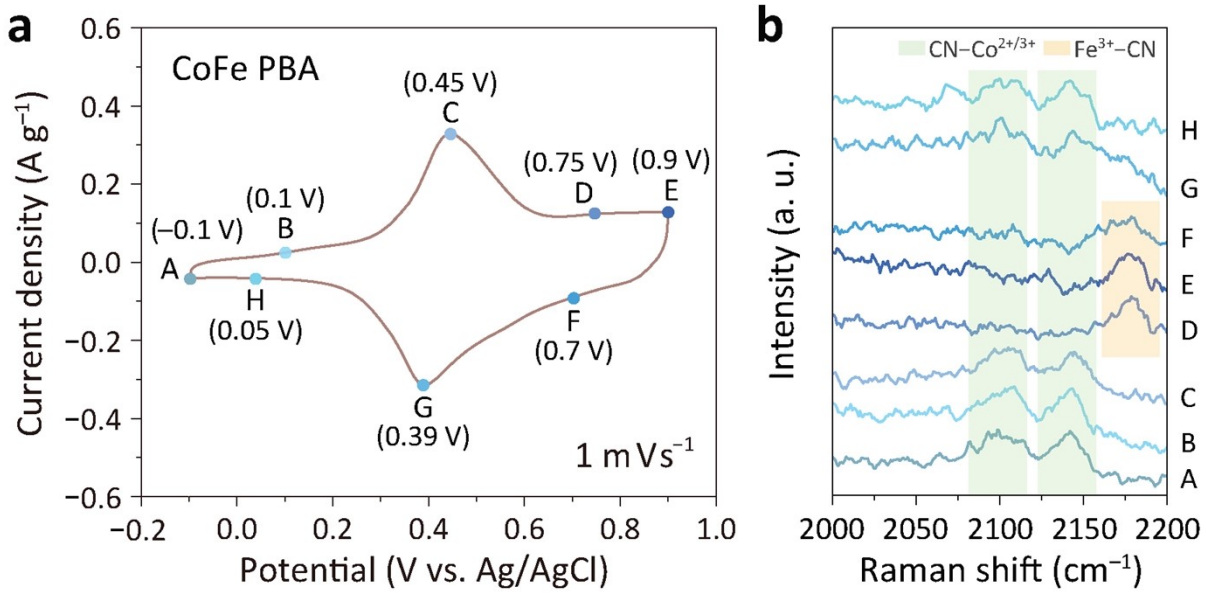

Fig. S6. (a) CV curve and (b) the related *in situ* Raman spectra of CoFe PBA at various applied potentials.

To better understand the energy storage mechanism in CoFe PBA, we have conducted *in situ* Raman spectroelectrochemical analysis with potential cycling between −0.1 and 0.9 V after the activation process in 0.5 M Na_2SO_4 electrolyte (**Fig. S6a**). The Raman spectra of CoFe PBA acquired at various applied potentials (**Fig. S6b**) exhibit the characteristic bands related to the two Na^+ intercalation/deintercalation processes that can be explained by the following equations:

$$Na_2Co^{II}[Fe^{II}(CN)_6] \leftrightarrow Na^+ + e^- + NaCo^{III}[Fe^{II}(CN)_6] \quad (1)$$

$$NaCo^{III}[Fe^{II}(CN)_6] \leftrightarrow Na^+ + e^- + Co^{III}[Fe^{III}(CN)_6] \quad (2)$$

When the voltage is applied in the anodic direction from −0.1 to 0.45 V (marked as A → C), two broad peaks that correspond to the valence states of the N-coordinated $Co^{2+/3+}$ species are observed at *ca*. 2,106 and 2,142 cm^{-1} (**Fig. S6b**, Eq (1)).[S1,2] Another peak assigned to the C-coordinated Fe^{3+} species appears at *ca*. 2,180 cm^{-1} in the high-potential region (0.75 and 0.9 V, marked as D → E) while the peaks for CN−Co species are suppressed (Eq. (2)).[S2] During the cathodic sweep from 0.7 to 0.05 V (F → H), the Fe^{3+}–CN band vanishes and the CN–Co bands re-emerges. This supports the reversible redox reactions on CoFe PBA.

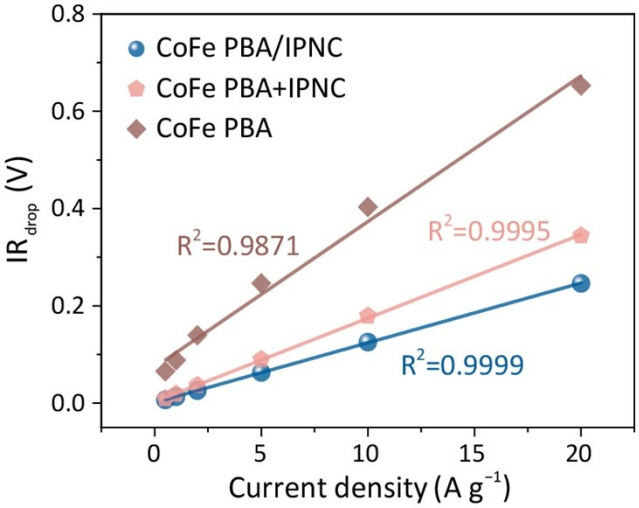

Fig. S7. Voltage drop (*i*R drop) of CoFe PBA/IPNC, CoFe PBA+IPNC, and CoFe PBA plotted as a function of current density from 0.5 to 20 A g^{-1}.

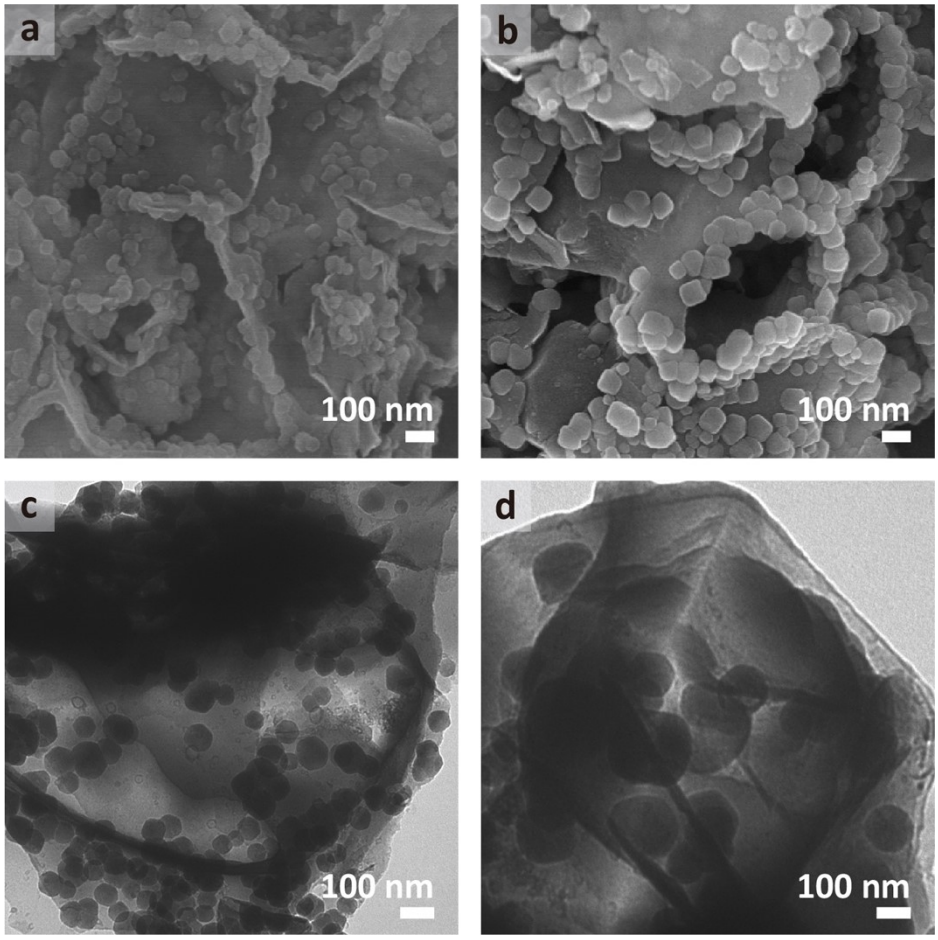

Fig. S8. SEM and TEM images of (a, c) CoFe PBA/IPNC-C1 and (b, d) CoFe PBA/IPNC-C2, respectively.

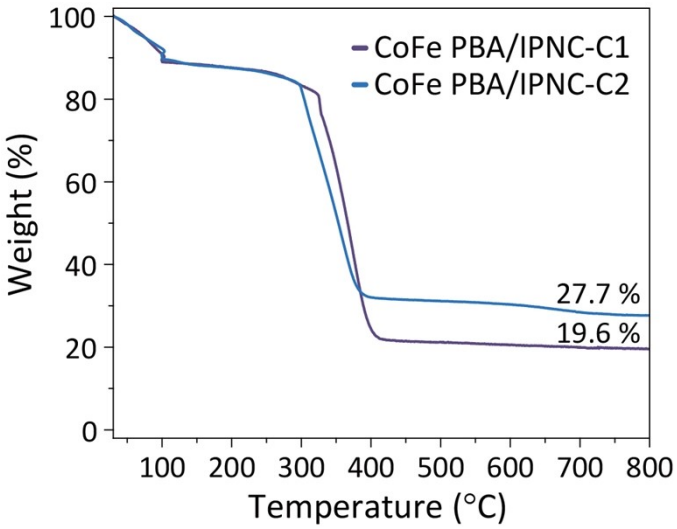

Fig. S9. Thermal gravimetric analysis (TGA) curves of CoFe PBA/IPNC-C1 and CoFe PBA-C2 obtained under an air atmosphere at a ramping rate of 10 °C min^{-1}.

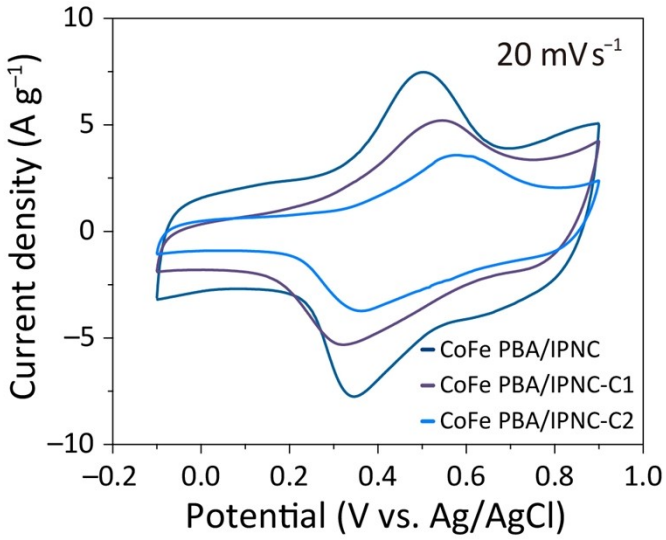

Fig. S10. CV curves of CoFe PBA/IPNC, CoFe PBA/IPNC-C1, and CoFe PBA/IPNC-C2 at a scan rate of 20 mV s^{-1}.

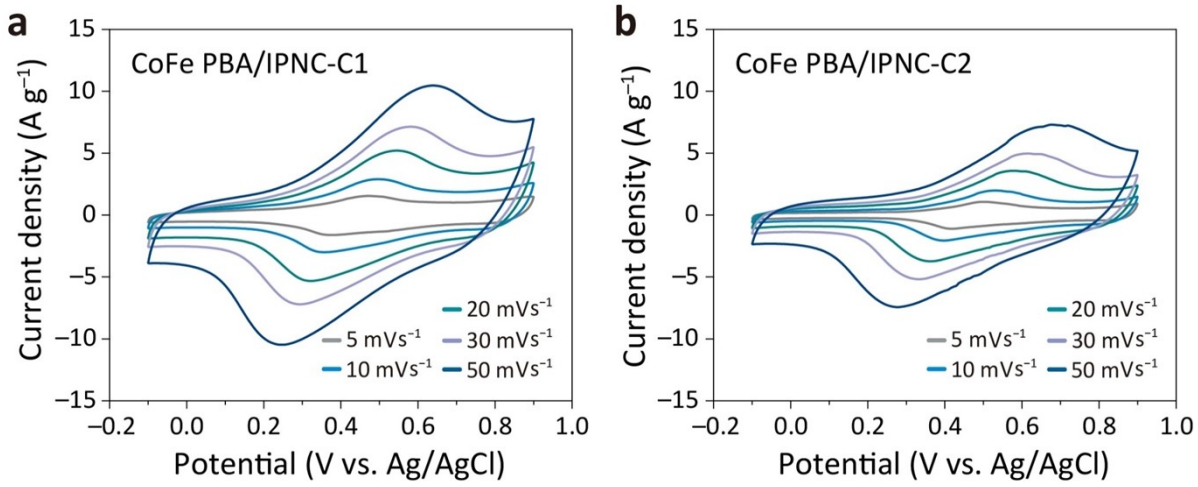

Fig. S11. CV curves of (a) CoFe PBA/IPNC-C1 and (b) CoFe PBA/IPNC-C2 at the various scan rates from 5 to 50 mV s^{-1}.

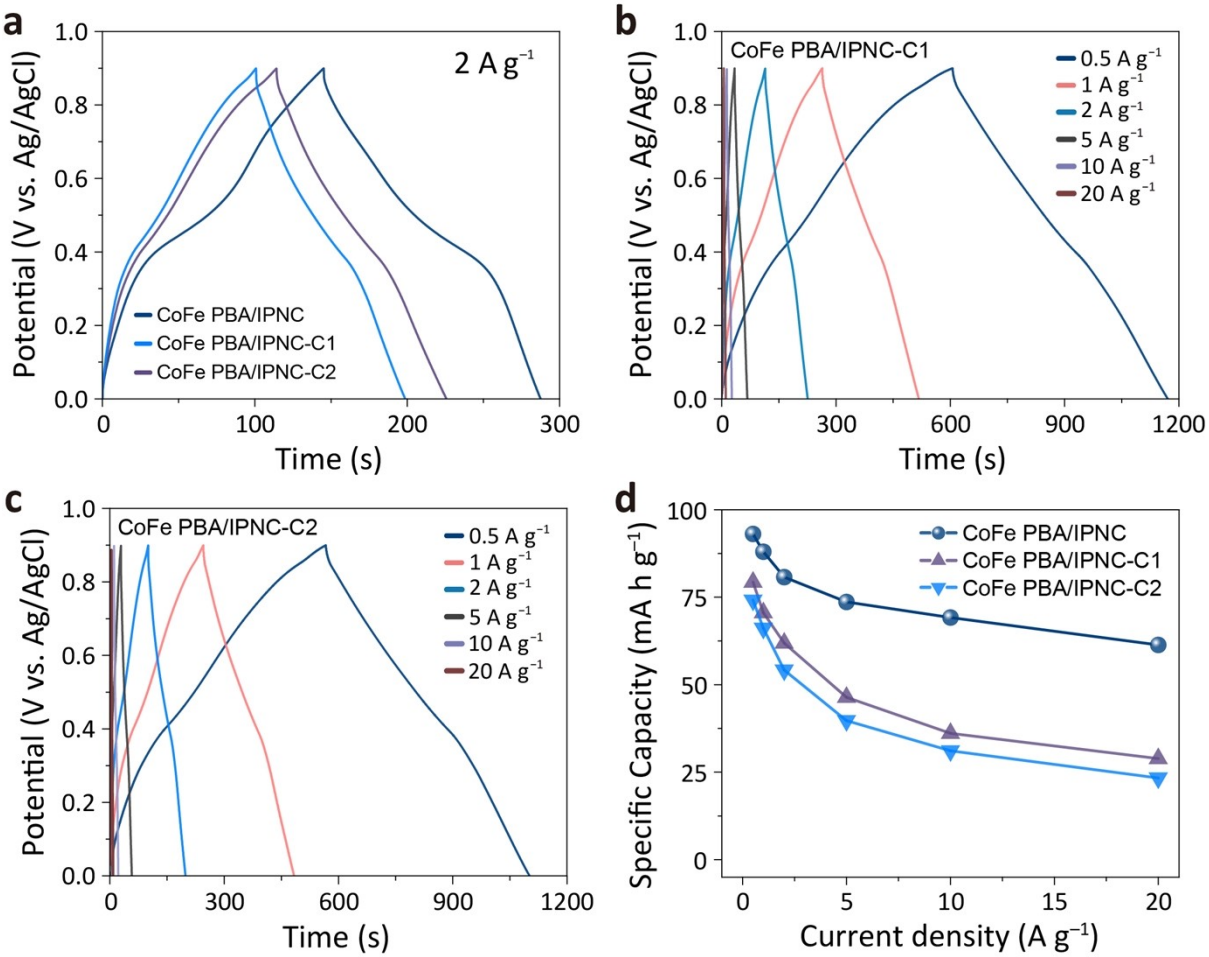

Fig. S12. (a) GCD profiles of CoFe PBA/IPNC, CoFe PBA/IPNC-C1, and CoFe PBA/IPNC-C2 at a current density of 2 A g^{-1}. GCD profiles of (b) CoFe PBA/IPNC-C1 and (c) CoFe PBA/IPNC-C2 at the different current densities range from 0.5 to 20 A g^{-1} and (d) the corresponding rate capabilities of CoFe PBA/IPNC, CoFe PBA/IPNC-C1, and CoFe PBA/IPNC-C2.

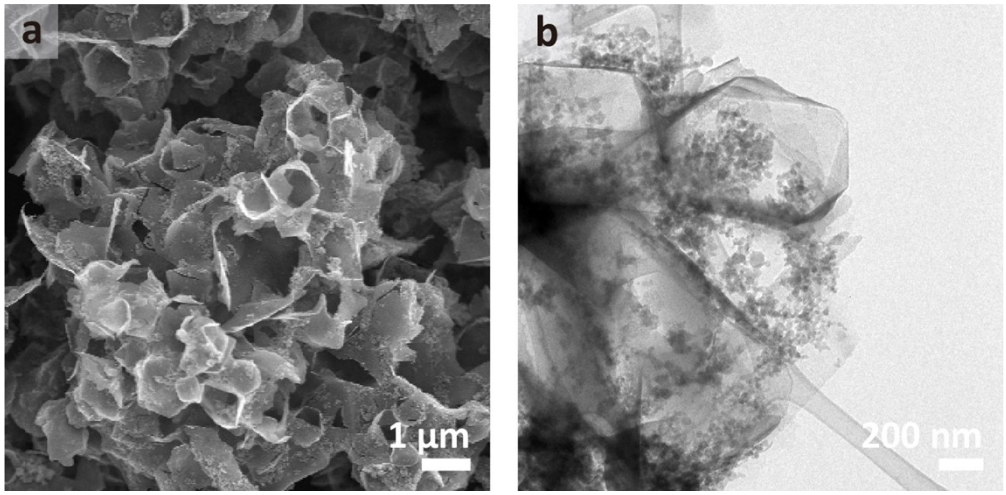

Fig. S13. (a) SEM and (b) TEM images of CoFe PBA/IPC.

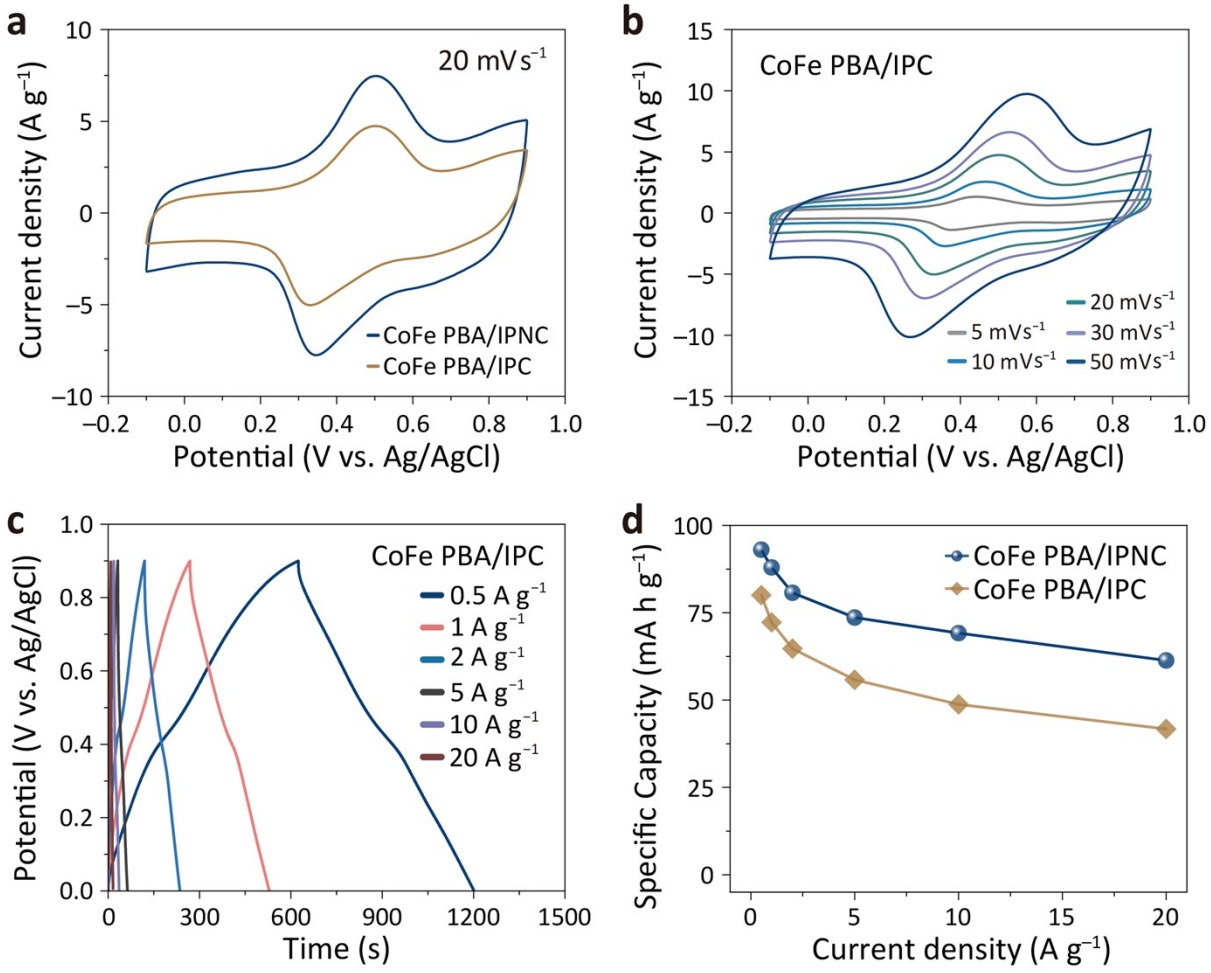

Fig. S14. (a) CV curves of CoFe PBA/IPNC and CoFe PBA/IPC at a scan rate of 20 mV s^{-1}. (b) CV curves of CoFe PBA/IPC at the different scan rates range from 5 to 50 mV s^{-1}. (c) GCD profiles of CoFe PBA/IPC at the different current densities range from 0.5 to 20 A g^{-1} and (d) the corresponding rate capabilities of CoFe PBA/IPC.

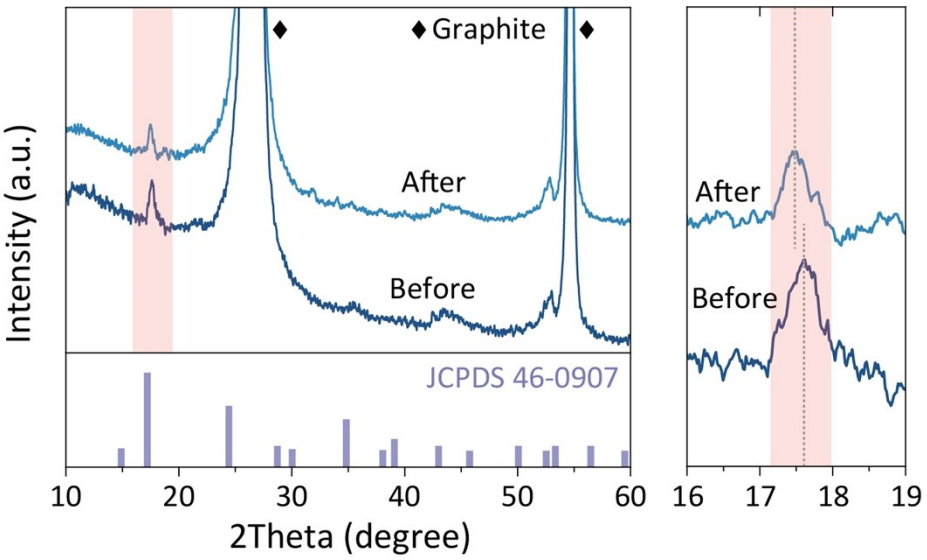

Fig. S15. XRD pattern of CoFe PBA/IPNC before and after 5,000 cycles.

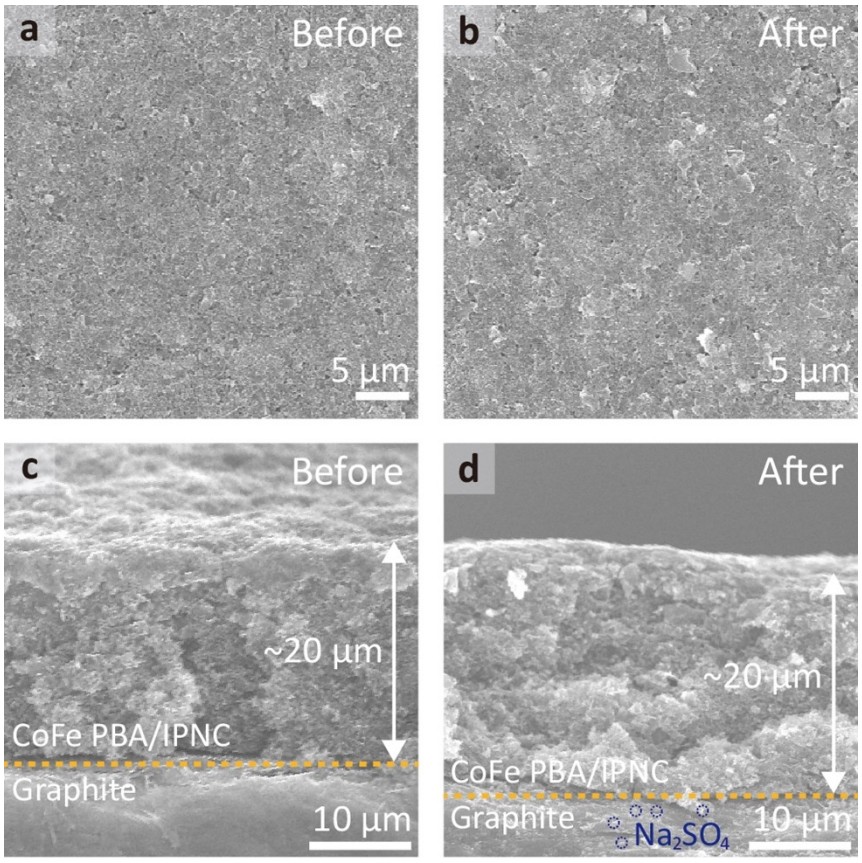

Fig. S16. (a, b) Top view and (c, d) cross-section of SEM images of CoFe PBA/IPNC electrode before and after 5,000 cycles.

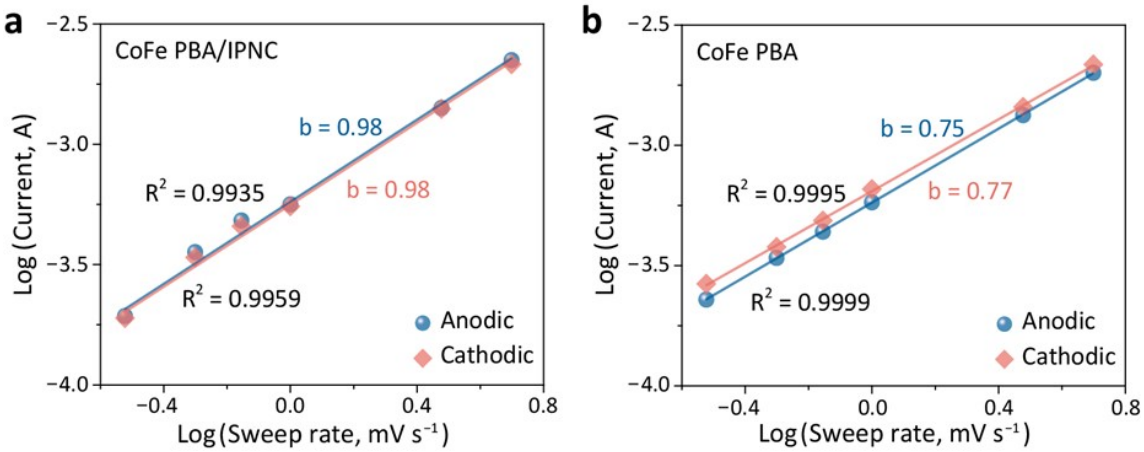

Fig. S17. Linear relationship between the redox peak current (*i*) and the scan rate (*v*) of (a) CoFe PBA/IPNC and (b) CoFe PBA electrodes.

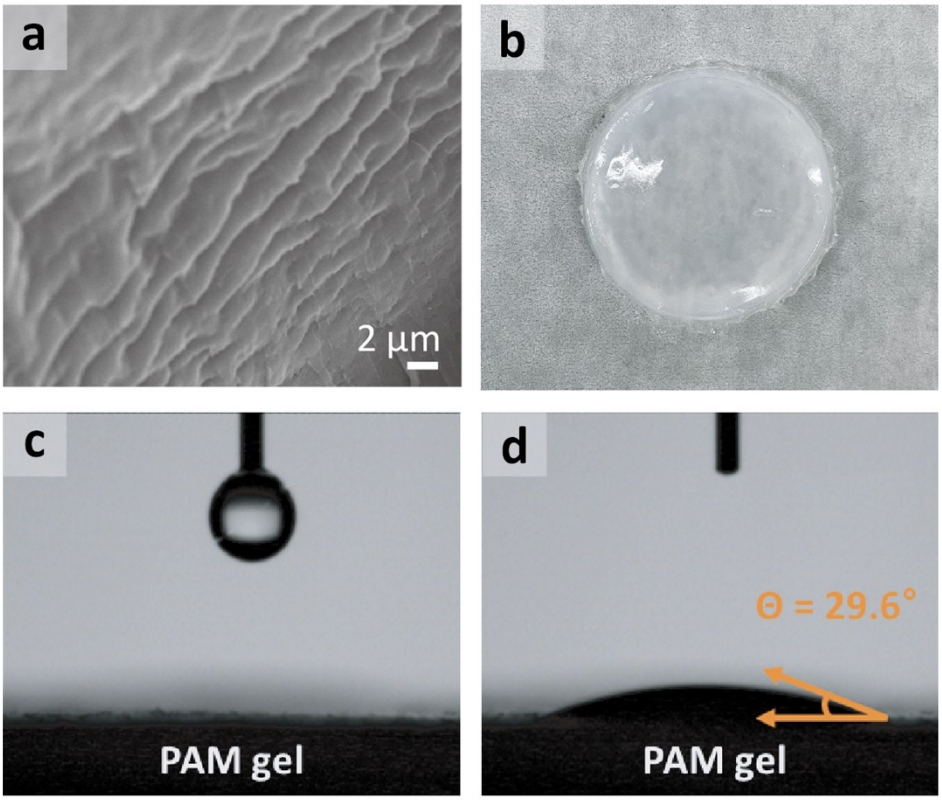

Fig. S18. (a) SEM image and (b) digital photo of PAM gel. (c, d) Water contact angle on the PAM gel substrate.

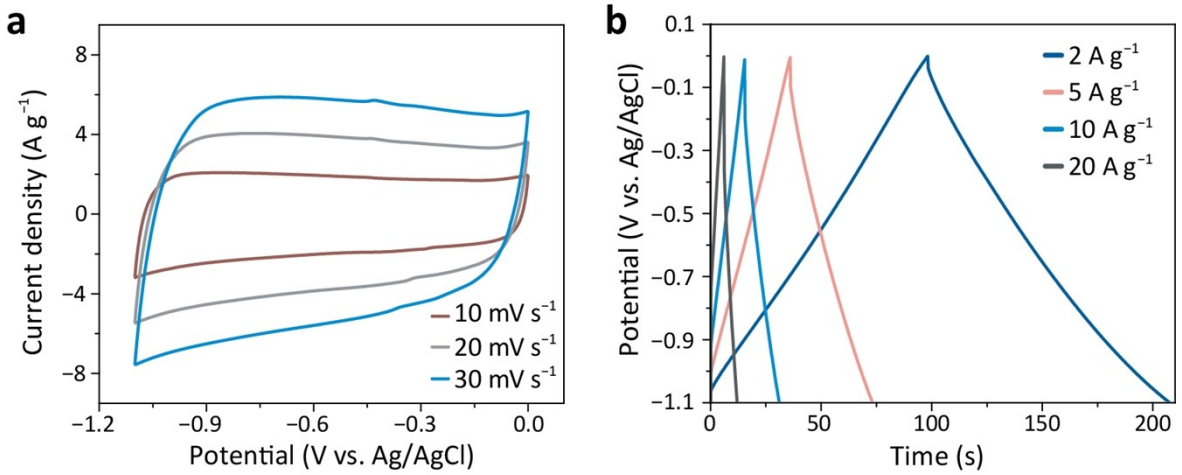

Fig. S19. (a) CV and (b) GCD curves of IPNC obtained in the voltage range of the negative electrode.

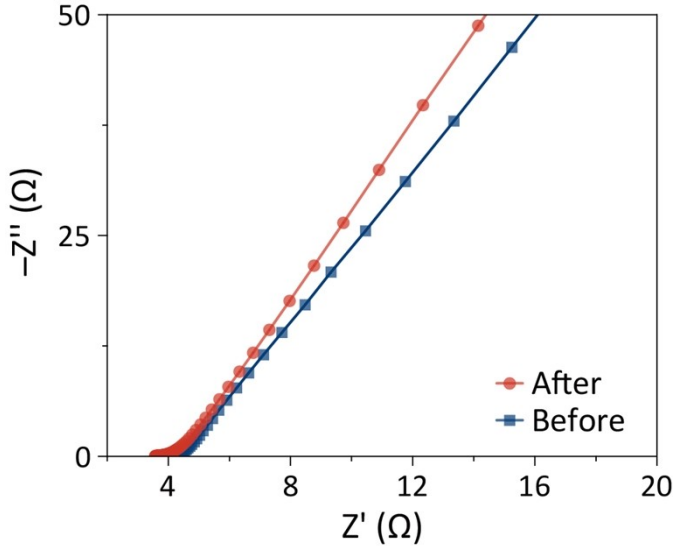

Fig. S20. EIS plots of full-device based on a gel electrolyte before and after the cycle test.

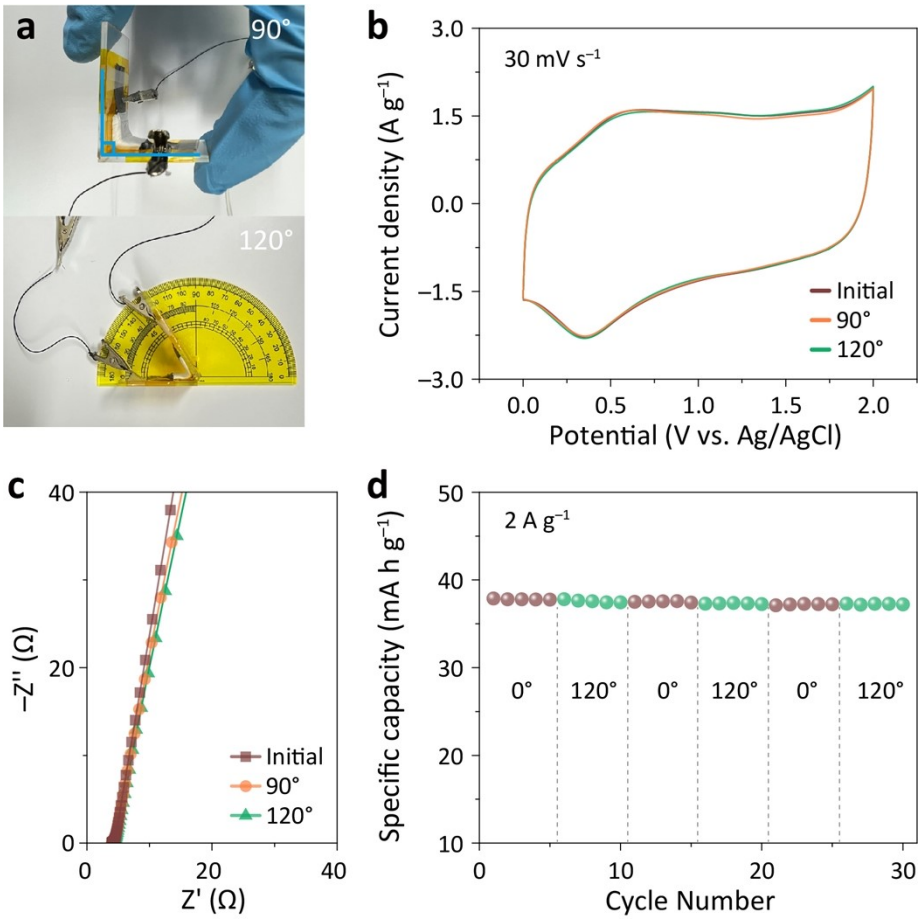

Fig. S21. (a) Photographs of the bent full-device (top: 90° and bottom: 120°). (b) CV curves of the full-device at a scan rate of 30 mV s^{-1} and (c) EIS plots obtained at different bending angles (0 to 120°). (d) Capacities of the full-device under the switcing mechanical conditions.

Table S1. Elemental analysis of IPC and IPNC.

Sample	Elemental composition (wt.%)			
	C	N	O	H
IPC	92.4	0	6.9	0.7
IPNC	90.4	4.5	4.3	0.8

Table S2. ICP analysis of CoFe PBA/IPNC and CoFe PBA.

Sample	Concentration of elements (ppm)		
	K	Co	Fe
CoFe PBA/IPNC	0.6	14.9	9.5
CoFe PBA	0.4	7	4.6

Table S3. Summary of the parameters used for EIS data analysis.

Sample	R_s (Ω)	R_{ct} (Ω)	W (Ω $s^{-1/2}$)	CPE (F)	C (F)
CoFe PBA/IPNC	4.77	3.22	429.83×10^{-3}	50.73×10^{-6}	206.88×10^{-3}
CoFePBA+IPNC	5.93	7.83	217.27×10^{-3}	27.74×10^{-6}	169.57×10^{-3}
CoFe PBA	7.42	51.25	2.89×10^{-3}	41.76×10^{-6}	625.6×10^{-6}

Table S4. Supercapacitor performances of CoFe PBA/IPNC electrode in comparison with recently reported electrodes (in 0.5 M Na_2SO_4).

Electrode	Three-Electrode			Hybrid capacitor		Ref.
	Potential (V *vs.* Ag/AgCl)	Specific capacity (Q_s) or capacitance (C_s)	Voltage (V)	E_{max} (Wh kg^{-1})	P_{max} (kW kg^{-1})	
PB/rGO†	−0.2 – 1	286 F g^{-1} at 0.3 A g^{-1}	0 – 2.0	45.4 (0.28 kW kg^{-1})	20.1 (18.2 Wh kg^{-1})	[S3]
Hollow CoHCF	0 – 1	292 F g^{-1} at 0.5A g^{-1}	0 – 2.0	42.5 (0.99 kW kg^{-1})	21.1 (13.5 Wh kg^{-1})	[S4]
CoHCF//mRGO	−0.1 – 1.1	250 F g^{-1} at 1A g^{-1}	0 – 2.4	34.4 (2.5 kW kg^{-1})	25 (6.7 Wh kg^{-1})	[S5]
rGO-NiHCF//SGC	0 – 0.8	294 F g^{-1} at 2 mV s^{-1}	0 – 1.8	25.4 (0.6 kW kg^{-1})	12 (7 Wh kg^{-1})	[S6]
CoHCF/rGO//AC	−0.1 – 1	340 F g^{-1} at 1A g^{-1}	0 – 2.0	39.6 (1 kW kg^{-1})	20 (1 Wh kg^{-1})	[S7]
MnHCF//Fe_3O_4/rGO†	0 – 0.8	238 F g^{-1} at 1 mA cm^{-2}	0 – 1.8	43.2 (0.27 kW kg^{-1})	2.18 (27.9 Wh kg^{-1})	[S8]
MnO_2@CNT†//MnO_3@CNT	−0.1 – 0.9	337 F g^{-1} at 1 mV s^{-1}	0 – 2.0	27.8 (0.52 kW kg^{-1})	9.8 (10 Wh kg^{-1})	[S9]
MnO_2/HCNFs	0 – 1	293.6 F g^{-1} at 0.5A g^{-1}	0 – 2.0	35.1 (0.5 kW kg^{-1})	8.78 (16.1 Wh kg^{-1})	[S10]
High-entropy PBA†	−0.2 – 1.0	175 F g^{-1} at 5 mV s^{-1}	-	-	-	[S11]
CoHCF†	0 – 1 (*vs.* SCE)	112 mAh g^{-1} at 0.5 C	-	-	-	[S12]
PB/MnO_2	0 – 0.8	623 F g^{-1} at 5 mV s^{-1}	-	-	-	[S13]
CoFe PBA/IPNC//IPNC	**0 – 0.9**	**93.1 mAh g^{-1} (372.2 F g^{-1}) at 0.5 A g^{-1}**	**0 – 2.0**	**42.9 (0.4 kW kg^{-1})**	**14.6 (15.5 Wh kg^{-1})**	**This work**

† 1 M Na_2SO_4 was used as the electrolyte.

References

[S1] H. Yang, J. Liu, Z. Chen, R. Wang, B. Fei, H. Liu, Y. Guo, R. Wu, *Chem. Eng. J.,* 2021, **420**, 127671.

[S2] R. Mažeikienė, G. Niaura, A. Malinauskas, *J. Electroanal. Chem.,* 2014, **719**, 60-71.

[S3] J. G. Wang, L. Ren, Z. Hou, M. Shao, *Chem. Eng. J.,* 2020, **397**, 125521.

[S4] J. G. Wang, Z. Zhang, X. Zhang, X. Yin, X. Li, X. Liu, F. Kang, B. Wei, *Nano Energy*, 2017, **39**, 647-653.

[S5] F. Zhao, Y. Wang, X. Xu, Y. Liu, R. Song, G. Lu, Y. Li, *ACS Appl. Mater. Interfaces*, 2014, **6**, 11007-11012.

[S6] Q. Zhou, T. Wei, Z. Liu, L. Zhang, B. Yuan, Z. Fan, *Electrochim. Acta*, 2019, **303**, 40-48.

[S7] J. G. Wang, Z. Zhang, X. Liu, B. Wei, *Electrochim. Acta*, 2017, **235**, 114-121.

[S8] K. Lu, D. Li, X. Gao, H. Dai, N. Wang, H. Ma, *J. Mater. Chem. A*, 2015, **3**, 1613-1619.

[S9] T. H. Lee, D. T. Pham, R. Sahoo, J. Seok, T. H. T. Luu, Y. H. Lee, Energy Storage Mater., 2018, **12**, 223-231.

[S10] P. Zhao, M. Yao, H. Ren, N. Wang, S. Komarneni, *Appl. Surf. Sci.* 2019, **463**, 931-938.

[S11] W. Jiang, T. Wang, H. Chen, X. Suo, J. Liang, W. Zhu, H. Li, S. Dai, *Nano Energy*, 2021, **79**, 105464.

[S12] T. Shao, C. Li, C. Liu, W. Deng, W. Wang, M. Xue, R. Li, *J. Mater. Chem. A*, 2019, **7**, 1749-1755.

[S13] X. Jin, S. Y. Son, M. G. Kim, S. J. Hwang, *Nano Energy*, 2020, **78**, 105255.